Carbonates and Evaporites (2020) 35:71
https://doi.org/10.1007/s13146-020-00606-4

ORIGINAL ARTICLE

Later fluid alteration of eogenetic karst spaces in carbonate: insights from the Cambrian Longwangmiao Formation, Northwestern Sichuan Basin, China

Xiaoxing Gong[1] · Zejin Shi[2,3] · Yaming Tian[4] · Xingui Zhou[1] · Wenjie Li[2,3] · Yong Wang[5]

Accepted: 3 June 2020 / Published online: 10 June 2020

Abstract

Pore-cave systems formed by karstification in the eogenetic stage of carbonate rocks provide abundant potential reservoir space for hydrocarbons. However, whether these dissolution pore-caves can become effective reservoir spaces during the later burial period, serving as the key to the success of hydrocarbon exploration. Therefore, it is important to explore the fluid activities and their alteration effects on eogenetic karst reservoirs during the later burial. Focusing on the Cambrian Longwangmiao Formation in the northwestern Sichuan Basin, this study systematically analyzed the formation of reservoir space in the eogenetic stage and the reworking of the system by fluids in the later stages, based on petrology, geochemistry, burial history, and tectonic evolution data. Results showed that many millimeters to several centimeters scale of pores and caves in the Longwangmiao Formation were produced by eogenetic karstification. These pore-caves underwent by two episodes of dolomite infilling in the shallow burial stage (D1) and in the Caledonian–Hercynian period (D2). Geochemical parameters indicate that D1 and D2 were both affected by meteoric water. In the early shallow burial stage, the dolomitic fluid was enriched in a relatively closed, reducing environment, whereas in the later stage, the fluid was affected by a relatively open oxidizing environment due to Caledonian–Hercynian fractures. Both D1 and D2 took place before the massive hydrocarbon migration from the Cambrian source rocks in the Middle Permian to those of the Middle Triassic. After the formation of the dissolution pore-caves, the precipitation from two episodes of dolomitic fluids led to the degradation of the Longwangmiao Formation carbonate reservoir space in the northwestern Sichuan Basin. In the southern part of the Shatan section-Well MS1, closed to the paleo-uplift of the central Sichuan Basin, where eogenetic karstification was superimposed by Caledonian–Hercynian supergene karstification, may be form effective reservoir and is a significant prospect for exploration.

Keywords Eogenetic · Karstification · Infilling · Longwangmiao formation · Sichuan basin

✉ Zejin Shi
zejin_shi@hotmail.com

✉ Yaming Tian
77837941@qq.com

[1] Oil and Gas Survey, China Geological Survey, Beijing 100083, China

[2] State Key Laboratory of Oil and Gas Reservoir Geology and Exploitation, Chengdu University of Technology, Chengdu 610059, China

[3] College of Energy Resources, Chengdu University of Technology, Chengdu 610059, China

[4] Key Laboratory of Tectonic Controls On Mineralization and Hydrocarbon Accumulation of Ministry of Natural Resources, Chengdu University of Technology, Chengdu 610059, China

[5] College of Earth Sciences, Chengdu University of Technology, Chengdu 610059, China

Introduction

Paleokarst reservoirs in carbonate rocks are an important target for hydrocarbon exploration and development and have achieved significant success (Budd et al. 1995; James and Choquette 1988; Loucks 1999; Zhao et al. 2014), such as the Puckett Oilfield of Lower Ordovician in west Texas (Loucks 1999), Emerald Oilfield of Silurian (Loucks 1999), Yates Oilfield of Permian (Craig 1988), Boonsville Oilfield of Lower Ordovician in the northern Fort Worth Basin (Hardage et al. 1996; McDonnell et al. 2007), and Madison Garland Oilfield of Mississippian in Wyoming (Demiralin et al. 1993). It is generally believed that the formation of karstic reservoirs is often controlled by the supergene or weathering crust karstification, which is typically related to unconformities (Moore 2001a). However, with

the development of hydrocarbon exploration, an increasing amount of carbonate pore-caves are being indentified that cannot be interpreted by the traditional theory of supergene or weathering crust karstification (Zhang and Liu 2009; White and Webb 2015; Xiao et al. 2016; Dan et al. 2018). For instance, in the Ordovician bioclastic limestone of the Honghuayuan Formation in the Sichuan Basin (Zhu et al. 2015), Cambrian dolomite in Well Tashen 1 (Zhu et al. 2012), and Ordovician carbonate in the Tazhong area of the Tarim Basin (Chen et al. 2016), there are many layered pores and/or caves in intervals with millimeters to several centimeters scale, developed within thick carbonate rocks, and they are not directly related to any unconformity surfaces. Further studies have found that these pores and caves are typically formed by short-term subaerial exposure due to a reduction in sea level in the syngenetic or penecontemporaneous period. Some scholars have defined this reworking as eogenetic karstification (Vacher and Mylroie 2002; Grimes 2006; Baceta et al. 2007; Cunningham and Florea 2009; Moore et al. 2010; Tan et al. 2015; Chen et al. 2016; Xiao 2017; Dan et al. 2018). Many of these karst reservoir spaces from the eogenetic stage are preserved in the late burial process, which is of great significance for hydrocarbon exploration. Therefore, the exploration of deep-buried, high-quality, carbonate reservoirs is very important for determine the influence of geological fluids on the reservoir spaces formed by eogenetic karstification and the types and mechanisms of fluid actions that occur during the late burial stages.

In 2012, there was a great breakthrough in the Cambrian Longwangmiao Formation in the Moxi area of central Sichuan Basin (Zou et al. 2014). The high-quality reservoir in the Longwangmiao Formation of central Sichuan Basin is dominated by fracture vug-type features, and the reservoir spaces consist mainly of dissolved pore-caves, which are formed by eogenetic karstification and superimposed by the Caledonian–Hercynian supergene karstification (Yang et al. 2015; Zhou et al. 2015; Zhang et al. 2015; Dai et al. 2016). However, the exploration for hydrocarbons in the Longwangmiao Formation has not revealed any discoveries, except in central Sichuan Basin. Therefore, there is a lack of detailed and systematic research, whereby the following questions arise: (1) is the Longwangmiao Formation in other areas of the Sichuan Basin affected by eogenetic karstification? (2) How has fluid altered the reservoir spaces formed by karstification in the eogenetic stage after burial? (3) Could the reservoir spaces have become a high-quality reservoir after reworking?

Therefore, in this study, a systematic analysis of the Cambrian Longwangmiao Formation in northwestern Sichuan Basin was performed, through the use of petrology and geochemistry analysis, combined with regional burial history and tectonic evolution history, to identify the characteristics of reservoir spaces produced by eogenetic karstification and explore the alteration processes and mechanisms by which the fluid activities are associated with these reservoir spaces during burial.

Geological setting

The Sichuan Basin is located in the northwestern margin of the Yangtze Block of southern China (Fig. 1a). The northern secetion of the Sichuan Basin is bounded by Micangshan mountain, with the Dabashan nappe structure to the east, the Longmenshan thrust structural belts to the west, and central Sichuan Basin to the south (Fig. 1b; Liu et al. 2014a; Yu et al. 2011). In the Early to Middle Cambrian, the topography of the Yangtze platform became flat. The Longwangmiao Formation in the Early Cambrian developed a shallow carbonate platform, distributed in the SE-NW direction (Fig. 1b; Feng et al. 2001, 2014; Ma et al. 2015; Ren et al. 2017). Influenced by the uplift of the northern and northwestern margin of the Sichuan Basin during the middle of the Early Cambrian (Gu et al. 2016), the Longwangmiao Formation in northwestern Sichuan Basin developed into a mixed tidal flat of carbonate rocks, including one third-order cycle and two fourth-order cycle sets (Fig. 2).

The Shatan section lies on the southern limb of the Shatan anticline (Fig. 1c, d; GPS: 32° 28′ 50″ N; 106° 52′ 59″ E), where the Longwangmiao Formation is well exposed, with a thickness of 122.40 m. An oolitic dolomite at the base is in contact with a quartz sandstone at the top of the underlying Yanwangbian Formation, whereas a silty dolomite seated at the top is in contact with an argillaceous siltstone at the base of the overlying Douposi Formation. The Longwangmiao Formation consists mainly of a set of restricted platform sedimentary sequences superimposed by shoal and dolomite flat microfacies. The lower part of the formation is inter-layered with crystalline and granular dolomite, whereas the upper part is thick layered gray silty dolomite (Fig. 2).

The Sichuan Basin has experienced Caledonian, Hercynian, Indosinian, Yanshan, and Himalayan orogenic cycles, which caused the sedimentary strata to undergo a complicated history of burial and uplift (Richardson et al. 2008; Liu et al. 2012; Rao et al. 2013). The hydrocarbon source rocks of the lower Cambrian strata began to enter into the oil generation window in the Early Silurian and followed into the mature stage in the Late Silurian. From the Late Silurian to the Carboniferous, the strata were uplifted and cooled, leading to the denudation of the lower Paleozoic strata, which led to the stagnation of the evolution of the lower Cambrian source rocks to stagnate. The strata then began to sink quickly during the Middle

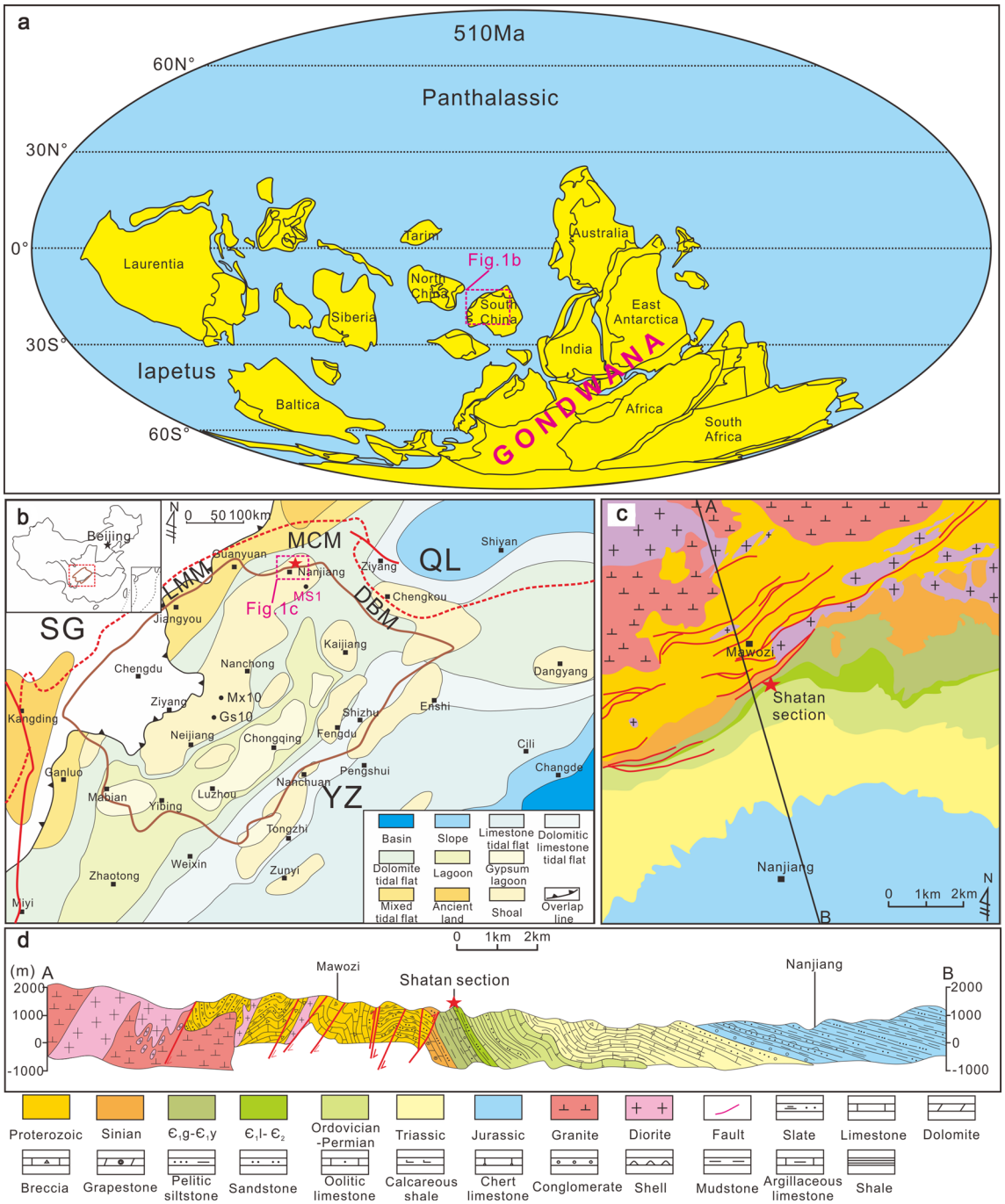

Fig. 1 Comprehensive geological map of the study area. **a** Paleogeographic reconstruction map for the Middle Cambrian is adapted from Torsvik and Cocks (2013); **b** sedimentary facies of the Longwangmiao Formation, Sichuan Basin; **c** geological map of the Shatan region in northwestern Sichuan Basin; **d** Geological section of the Shatan in northwestern Sichuan Basin. *SG* Songpan-Garze flysch, *QL* Qinling Orogen, *YZ* Yangtze Block, *LMM* Longmenshan Mountains, *MCM* Micangshan Mountains, *DBM* Dabashan Mountains, $Є_1g$–$Є_1x$ Guojiaba Formation–Xiannüdong Formation, $Є_1l$–$Є_2$ Longwangmiao Formation–Middle Cambrian

Permian. In the Early Triassic, the lower Cambrian source rocks gave rise to secondary hydrocarbon generation. The Middle Permian to Middle Triassic was the peak period of oil generation for the lower Cambrian source rocks, in which hydrocarbons migrated to the top of the uplift and/or slope to form a paleo-oil reservoir (Richardson et al. 2008; Liu et al. 2012) (Fig. 3).

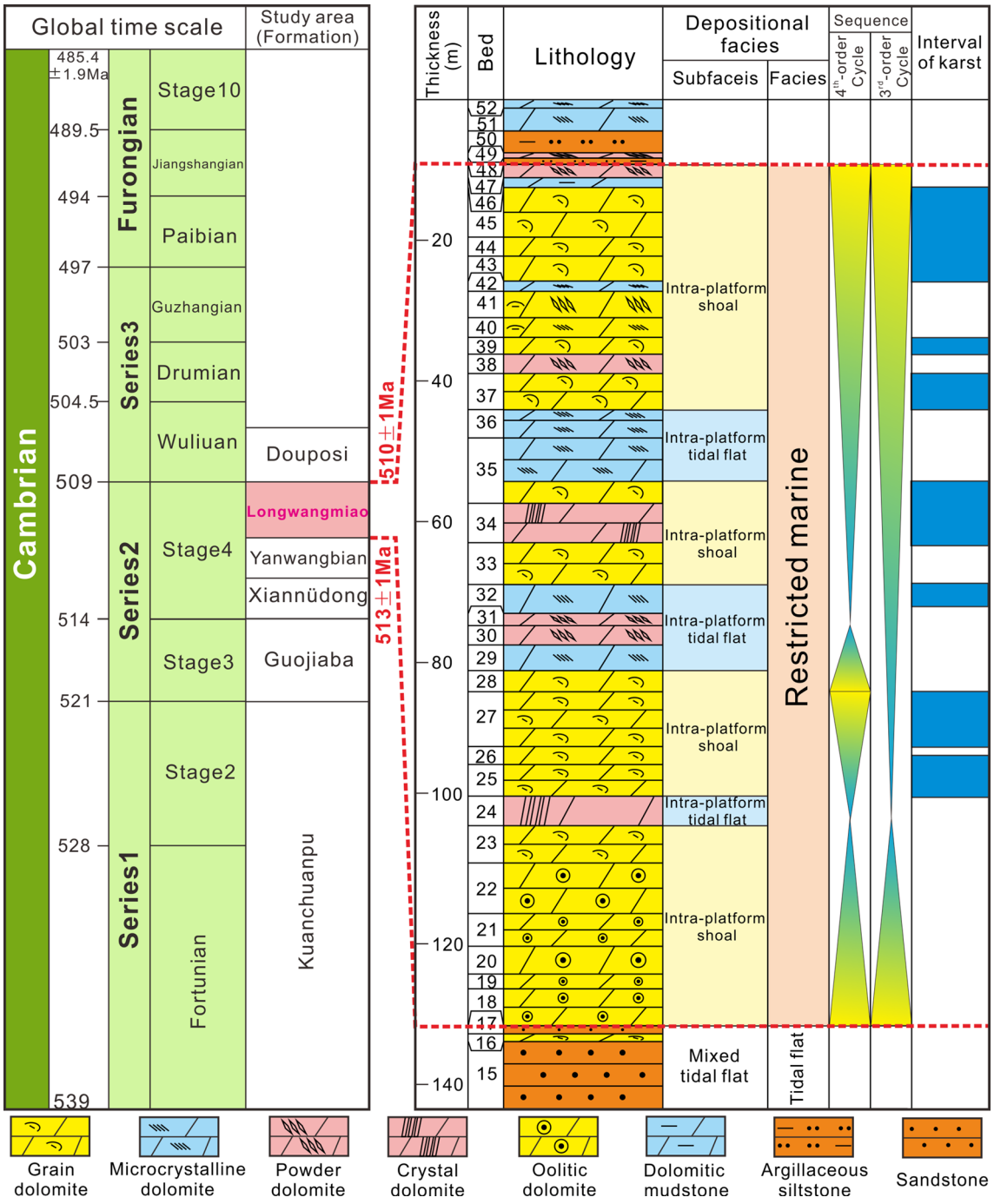

Fig. 2 Comprehensive stratigraphic column of the Longwangmiao Formation, northwestern Sichuan Basin (Cambrian stratigraphic sequence is derived from Zhu et al. 2006. The chronological information for the top of the Longwangmiao Formation is derived from Ren et al. 2017)

Samples and methods

Samples

The samples used in this study were collected from the Shatan section and Well MS1 (Fig. 1b). A total of 160 samples underwent double-sided polishing and were prepared as thin sections with no cover slips. These thin sections were impregnated with blue epoxy for mineralogical analysis. A total of 80 pore-cave infillings and host rock samples were extracted using a micro-drill, washed with deionized water, and ground with an agate mortar into a powder of size less than 0.0750 mm in preparation for geochemical analysis. All processing and testing of samples were performed at

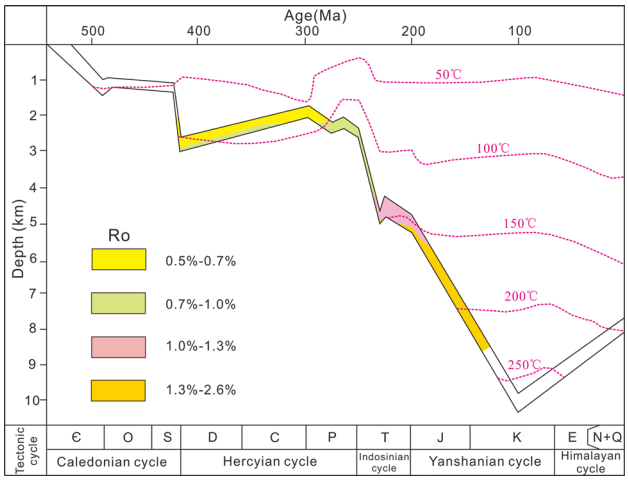

Fig. 3 Burial history of northwestern Sichuan Basin (Well MS1)

the State Key Laboratory of Oil and Gas Reservoir Geology and Exploitation of Chengdu University of Technology, Chengdu, China.

Methods

In this examination, 160 thin sections were examined using a Nikon ECLIPSE LV100POL polarizing microscope. Selected polished thin sections were examined with cathodoluminescence (CL) microscopy. The CL observations were performed using a CL8200MK5 cold-cathode device coupled with a Leica DM2500 digital photographic system. The operating conditions for the CL analyses were set at an acceleration voltage of 12 kV and beam current of 300 μA.

Selected polished thin sections were used to conduct in-situ analysis of major and trace elements, with an EPMA-1720 electron microprobe equipped with a backscattered electron detector (BSE). The operating conditions were set at an acceleration voltage of 20 kV and beam current of 10–15 nA. The standard materials for each element are listed as follows: albite for Na, potassium feldspar for K, magnetite for Fe, celestite for Sr, dolomite for Mg, calcite for Ca, MnO for Mn, barite for Ba, almandine for Al, and SiO_2 for Si, with a resolution limit of 0.002%.

For each analysis of carbon and oxygen stable isotope, 0.5 mg of a sample was placed in a tube of the GasBench automatic sampling system, cleaned with high-purity helium, and dissolved with 100% H_3PO_4 at 25 °C for 2 h. The $\delta^{13}C$ and $\delta^{18}O$ values were measured using a Thermo Fisher Scientific MAT253 isotope mass spectrometer at a temperature of 25 °C and humidity of 50%. During the test, the standard samples (ANU-M_1, ANU-M_2, ANU-PRM_2, GBW04405) and blank samples were used to control the quality. The mean measured $\delta^{13}C$ and $\delta^{18}O$ of standard ANU-M_1 ($\delta^{13}C=+1.34\pm0.01‰$, $\delta^{18}O=-6.16\pm0.04‰$, $n=4$), ANU-M_2 ($\delta^{13}C=+2.82\pm0.02‰$, $\delta^{18}O=-7.32\pm0.03‰$, $n=2$), ANU-PRM_2 ($\delta^{13}C=+0.73\pm0.03‰$, $\delta^{18}O=-17.42\pm0.04‰$, $n=3$), GBW04405 ($\delta^{13}C=+0.57\pm0.02‰$, $\delta^{18}O=-8.57\pm0.04‰$, $n=5$), were consistent with their recommended values (ANU-M_1: $\delta^{13}C=+1.36\pm0.12‰$, $\delta^{18}O=-6.14\pm0.11‰$, ANU-$M_2$: $\delta^{13}C=+2.81\pm0.17‰$, $\delta^{18}O=-7.34\pm0.08‰$, ANU-$PRM_2$: $\delta^{13}C=+0.71\pm0.21‰$, $\delta^{18}O=-17.41\pm0.19‰$, and GBW04405: $\delta^{13}C=+0.57\pm0.03‰$, $\delta^{18}O=-8.49\pm0.14‰$). Isotope values are reported relative to the Pee Dee Belemnite (PDB) standard, whereby the analysis precision of $\delta^{13}C$ is better than 0.03‰, and that of $\delta^{18}O$ is better than 0.04‰.

For each analysis of strontium isotopes, 50 mg of a sample was dissolved using 1 M ultrapure acetic acid for approximately 12 h on an electric hot plate at 60 °C. A pure 1.5 mL solution was extracted after adding 1.5 mL 2.5 M HCl. The Sr purification and separation of Rb and other cations, such as Ca^{2+} and Ba^{2+}, was performed using AG 50 W × 12 cation exchange resin. Ratios of $^{87}Sr/^{86}Sr$ were then measured using a Thermo Fisher Scientific TRITON Plus Mass Spectrometer. The measured $^{87}Sr/^{86}Sr$ ratios were normalized to an $^{86}Sr/^{88}Sr$ ratio of 0.1194 and then calculated from 150 measurements. Analytical precision was normalized by analysis of the NBS-987 standard. The mean measured $^{86}Sr/^{88}Sr$ ratios of the NBS-987 standard was 0.710255 ± 0.000008 ($n=3$), which was consistent with its recommended value ($^{87}Sr/^{86}Sr=0.710246\pm0.000042$). All sample data have been adjusted to an assumed NBS-987 value of 0.710250.

A PerkinElmer SCIEX ELAN DRC-e inductively coupled plasma mass spectrometer was used for trace elements and rare earth elements (REEs) analyses. For each analysis, 0.1 g of powdered sample was dissolved in a Teflon bomb using ultrapure hydrochloric acid on an electric hot plate at 180 °C for 48 h. After the solution was centrifuged and evaporated, the sample was re-dissolved by adding 1.5 mL ultrapure nitric acid and heated at 140 °C for 6 h. The final pure solution was diluted to 100 g with a mixture of 2% nitric acid for analysis. USGS rock standards and Chinese national rock standards GSD-1, GSR-2, GSR-3, and GSR-9 were used to calibrate the elemental concentrations of the measured samples. The analytical errors were less than 5%. The sample preparation procedure for the major elements is the same as that for the trace elements and REEs, measured by ICP-OES (PE 5300 V). Analytical accuracies are estimated to be ±2%.

Results

Characteristics of syngenetic karstification in the eogenetic stage

The karst interval in the Longwangmiao Formation of the Shatan Section was developed in the middle and upper

parts of the shoal and dolomite flat microfacies (Fig. 2). The dissolution pore-caves are mainly concentrated in the strata of the grain and fine-microcrystalline dolomite. They are developed in Beds 25, 27, 28, 32, 34, 35, 37, 39, and 43–45, but are relatively undeveloped in the strata with high argillaceous contents. The karst interval in Bed 25 is ~4.5 m thick, Bed 27–28 is 10.8 m, Bed 32 is 4 m, Bed 34–35 is 8 m, Bed 37 is 3 m, Bed 37 is 2 m, and Bed 43–45 is 13.3 m, such that the total thickness of the karst interval is ~45.3 m (Fig. 2). Most of the dissolved pores are distributed near the top surface of the layer and distributed horizontally along the layer (Fig. 4a, b). An erosion feature is apparent in the upper part of the dissolved pores, which shows that the formation of dissolved pores is related to the horizontal hydrodynamic force. Calcareous laterite, which is approximately 0.1–0.5 cm in thickness (Fig. 4c), occurs at the surface, and has significant exposure characteristics. The dissolved pores of the Shatan section are elliptical in shape with uneven distribution, whereas the size of the pore-caves is approximately 0.5–2 cm (Fig. 4a, b, d, f). The karst interval of Well MS1 (depth: 7289–7402 m) occurs mostly as needle-like dissolution pores (Fig. 4f) that are 1–10 mm in size and are densely distributed. The pore-caves in outcrop and well strata are all filled, in whole or in part, with dolomite (Fig. 4a, b, d, f).

Choquette and Pray (1970) subdivided the postdepositional evolution of the carbonate porosity into three time-porosity stages conforming to the rock cycle. They defined the time of early burial as "eogenetic", the time of deeper burial as "mesogenetic", and the late stage associated with erosion of long-buried carbonates as "telogenetic". Vacher and Mylroie (2002) first used the term "eogenetic karst" for the land surface evolving on and the pore system developing in rocks undergoing eogenetic, meteoric diagenesis. Based on the traditional classification of eogenetic karst (i.e., syngenetic karst and penecontemporaneous karst), Xiao (2017) considered the level of sequence boundary and exposure time of syngenetic and penecontemporaneous karst, and

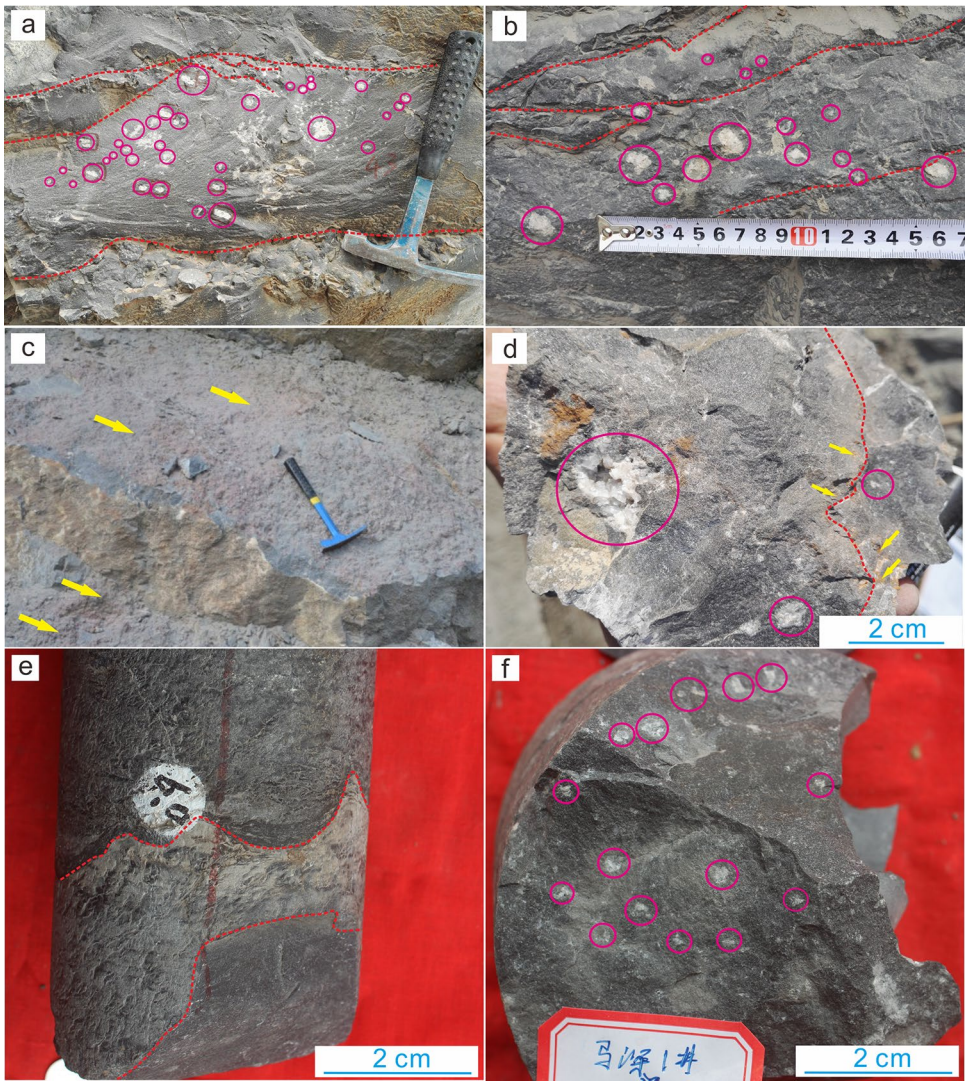

Fig. 4 Karst characteristics of the Longwangmiao Formation, northwestern Sichuan Basin. **a** Dissolution pore-caves and erosion surface of the upper Longwangmiao Formation, fully filled with dolomite, Bed 43 in Shatan section; **b** dissolution pore-caves and erosion surface of the middle Longwangmiao Formation, Bed 25 in Shatan section; **c** calcareous laterite at the surface of the Longwangmiao Formation, Bed 34 in Shatan section; **d** dissolution pore-caves of the middle Longwangmiao Formation, fully or partly filled with dolomite, Bed 25 in Shatan section; **e** erosion surface at 7302.30 m in Well MS1; **f** needle-like dissolution pore-caves, fully filled with dolomite, at 7302.30 m in Well MS1. The red line represents the erosion surface; the pink circle indicates the solution pores or caves; the yellow arrow indicates the calcareous laterite, and the geological hammer is 28 cm long

defined the syngenetic karst strictly controlled by the fourth- to sixth-order sequence (0.01–0.5 Ma) boundary. The object of karstification is synsedimentary, which was dominated by the transformation of the matrix pores and generally did not exhibit "diachronous" characteristics. The Lower Cambrian Longwangmiao Formation is conformable overlain by thick Middle Cambrian Douposi Formation in the northwestern Sichuan Basin. After the deposition of the Longwangmiao Formation, it did not experience exposure or denudation, thus, there is no direct relationship between the dissolved pore-caves with several millimeters to several centimeters scale in the Longwangmiao Formation and any unconformity surface. In other words, it is not a supergene karst. In addition, these dissolution pore-caves show a clear distribution along the horizontal plane and are associated with irregular scoured surfaces (Fig. 4). The irregular scoured surfaces are the product of erosion resulting from the exposure of the strata due to a temporary fall in relative sea-level during the depositional period. Very thin layers of calcareous clay also indicate sediment exposure and subsequent weathering processes (Hardie et al. 1986; Nicolas et al. 2012; Zhu et al. 2018). The characteristics of a small-scale pore-cave associated with scoured surfaces in the Longwangmiao Formation indicate that it is mainly controlled by short-term exposure of sediments, which are caused by the reduction in the sea level during the depositional period. In the syngenetic stage, the strata occur in a relatively shallow aqueous environment and would be exposed by a short-term sea-level fall. Because the sediments are not consolidated and the carbonate mineral fabric is not stable, it is readily affected by meteoric water to be dissolved. However, owing to the shortness of the exposure and the limited scale of dissolution, the pore-caves are millimeters to centimeters in size. Episodic sea-level changes during the syngenetic stage will lead to repeated exposure of the strata, in which multi-layer karst intervals are formed in the Longwangmiao Formation.

Characteristics of pore-caves infilling

Petrology and sequence of pore-caves infilling

The small karst pore-caves formed by syngenetic karstification in the Longwangmiao Formation are filled with dolomite. The CL image features of dolomite infilling are different from that of the host rock. The dolomite infilling in the dissolution pore-caves that were formed during the syngenetic stage exhibit two types of luminescence. The host dolomite (D0) is characterized by a dark red-red luminescence. The dolomite that glows dark red is from the first period of infilling (D1), whereas the dolomite that glows bright red is from the second (D2) (Fig. 5a, b). The D2 is usually related to tensile fractures, and the CL characteristics of the D2 in the dissolution pore are consistent with that of dolomite infilling in the tension fracture, showing continuous filling of dissolution pore-caves formed in the syngenetic stage. Macroscopically, the fractures generally shown an echelon pattern, with a fracture dip angle between 70°and 85°; meanwhile, the width of the fracture varies significantly between 2 and 8 mm (Fig. 5c, d). After two episodes of dolomite infilling, most of the dissolution pore-caves that formed in the syngenetic stage were infilled compactly, although occasionally they were infilled with organic matter (Fig. 5e).

The characteristics of the outcrop, thin section, and CL images show that the sequence of formation and infilling of the dissolution pore-caves is as follows: (1) dissolution pores formed during the syngenetic period; (2) dissolution pore-caves were infilled by D1; (3) tension fractures formed; (4) the dissolution pore-caves and fractures were infilled by D2; and (5) remnant dissolution pore-caves were filled by organic matter.

Geochemical characteristics of the pore-cave infilling

Major and trace elements The CaO contents of D0, D1, and D2 are 28.785–31.269%, 28.381–30.856%, 29.555–30.567%, and the MgO contents are 18.822–20.789%, 20.636–21.204%, 20.365–21.023%, respectively. The results indicated that the host rock and two episodes of infilling were relatively consistent of CaO and MgO, which were dolomite. The D0 has higher Na, K, and Ba contents, lower Sr and Mn contents, and relatively lower Fe content relative to the two episodes of dolomite infilling. D1 shows the characteristics of higher Fe and Sr contents, lower Na contents and relatively lower K, Mn, and Ba contents. Meanwhile, D2 has higher Mn content, lower Fe, Ba, and K contents, and relatively lower Na and Sr contents (Table 1).

The characteristics in outcrop, microscopy, and CL indicate that the two episodes of dolomite infilling in the karst pore-caves have distinct differences. In this study, the two episodes of dolomite and the host rock were selected for in-situ EPMA analysis (Fig. 6). The data of in-situ EPMA analysis show that D0 has higher Na_2O, K_2O, and BaO contents, lower MnO content, and relatively lower FeO content, compared with the two episodes of dolomite infilling. D1 show the characteristics of higher FeO and SrO contents, lower Na_2O content, and relatively lower MnO content, whereas D2 has higher MnO content, lower FeO and K_2O contents, and relatively lower Na_2O content. Overall, the data of the major and trace elements in the whole rock and the in-situ EPMA analysis match with good consistency (Table 2).

Rare earth elements The range of variation and mean value of total rare earth elements (ΣREE) in D0 and D1 show no difference and is lower than that of D2. The $(Nd/Yb)_{SN}$ of carbonate rocks can be used as a parameter to judge the relative enrichment of light (LREE) or the heavy

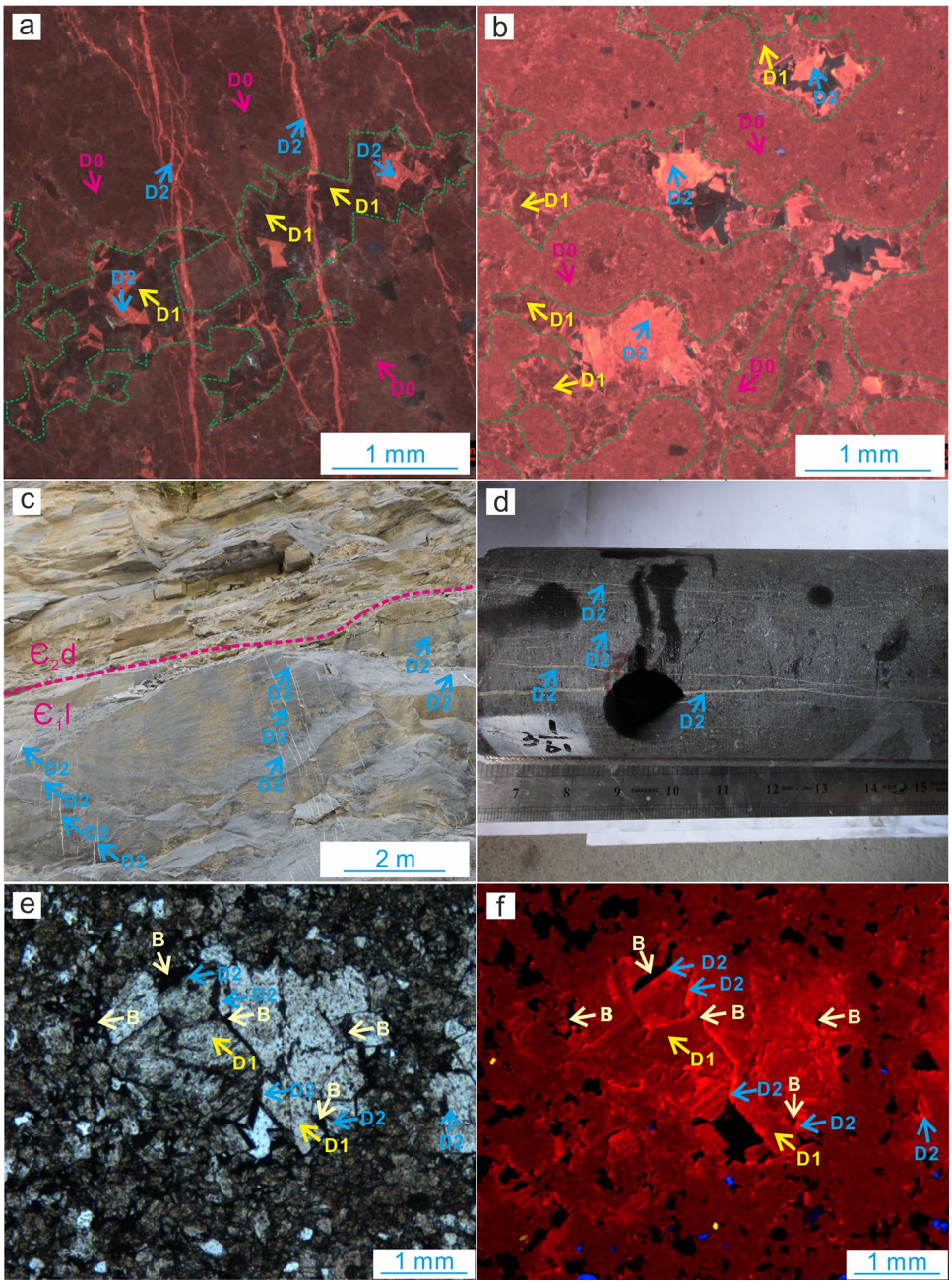

Fig. 5 Characteristics of the karst infilling of the Longwangmiao Formation, northwestern Sichuan Basin. **a** CL characteristics of two episodes of karst pore-cave dolomite infilling, Bed 21 in Shatan section; **b** residual oolitic dolomite. The dissolution pore-caves are fully or partly filled by the second episode of dolomite, Bed 44 in Shatan section; **c** the high-angle fracture in the Longwangmiao Formation is in an en echelon pattern, and is fully filled with dolomite, Bed 47 in Shatan section; **d** the high-angle fracture is filled with dolomite, at 7297.27 m in Well MS1; **e** features of the pore-caves infilling, at 7302.49 m in Well MS1; **f** CL characteristics of the dissolution pore infilling in the same view as **e**, at 7302.49 m in Well MS1. The green line indicates the edge of the dissolution pore-caves; pink arrow indicates matrix dolomite (D0); yellow arrows indicate the first dolomite infilling (D1); blue arrows indicate the second dolomite infilling (D2); light yellow arrows indicate organic matter infilling. $\epsilon_1 l$ Longwangmiao Formation, $\epsilon_2 d$ Douposi Formation, *B* bitumen

rare earth elements (HREE) (Nothdurft et al. 2004). The mean $(Nd/Yb)_{SN}$ value in D1 is 3.010 (2.529–3.469), compared with D0, the LREE is relatively enriched, and HREE is relatively deficient, demonstrating considerable differentiation between LREE and HREE. In contrast, the LREE and HREE of D2 show only weak differentiation. The mean δEu value in D1 is 2.272 (1.827–2.930), which has strong Eu positive anomaly, and the mean value of δCe is 0.862 (0.844–0.888), which is a weaker negative anomaly than that of D0. δEu and δCe in D2 are similar to those of D0 (Table 3).

Carbon and oxygen isotopes The value of $\delta^{13}C$ in D0 of the Longwangmiao Formation ranges from −1.40 to +0.64‰, with a mean value of −0.36‰. The $\delta^{13}C$ value of the D1 ranges from −1.03 to +0.41‰, with a mean value of −0.18‰. The value of $\delta^{13}C$ of D2 ranges from −1.22 to −0.29‰, with a mean value of −0.96‰ (Table 4). There is no significant difference in the carbon isotope compositions between D0 and D1; however, the values of D2 is lighter than those of D0 or D1. For D0, the value of $\delta^{18}O$ ranges from −6.86 to −4.89‰, with an average of −6.07‰, whereas the oxygen isotope compositions of the two epi-

Table 1 Major and trace elements of the host dolomite and two episodes of dolomite infilling of the Longwangmiao Formation, northwestern Sichuan Basin

Type	Section/well	Bed/depth	Sample	Na (ppm)	K (ppm)	Sr (ppm)	Fe (ppm)	Mn (ppm)	Ba (ppm)	CaO (wt%)	MgO (wt%)
D0	MS1	7297.85 m	M1w	421.86	3323.24	51.67	2886.86	124.25	43.18	30.067	19.43
	Shatan	27	NJ-27-0C	233.6	3725	29.69	4043	353	24.26	29.475	19.575
	Shatan	39	NJ-39-1C	117.01	1262.87	48.94	6511.76	314.96	26.42	30.879	20.285
	Shatan	34	NJ-34-00C	259.7	7768	62.64	4352	409.29	34.57	31.269	18.822
	Shatan	32	NJ-32-1C	242.1	2829	42.22	2786	292.61	50.78	30.348	20.406
	Shatan	25-2	NJ-25-2C	212.59	2811.89	28.18	10,569.04	378.25	16.33	29.124	20.007
	Shatan	25-1	NJ-25-1C	175.7	2990	20	4813	87.89	75.93	28.785	20.789
	–	–	Mean ($n=7$)	237.51	3530	40.48	5137.38	280.04	38.78	29.992	19.902
D1	Shatan	25-2	NJ-25-2d	50.05	33.02	125.24	10,917.3	340.45	1.49	28.381	21.204
	Shatan	25-1	NJ-25-1d	115.5	188.4	128.71	6525	344.21	3.43	30.764	20.861
	Shatan	27	NJ-27d	248.2	4098	122.03	5208	412.89	59.7	30.036	20.829
	Shatan	34	NJ-34-00d	144.1	450.8	322.71	5938.7	536.19	18.23	30.856	20.636
	Shatan	34	NJ-34-1d	155	642	200.92	5174.1	204.66	24.18	29.546	21.159
	–	–	Mean ($n=5$)	142.57	1082.44	179.92	6752.62	367.68	21.41	29.916	20.939
D2	MS1	7297.85 m	M1m	287.28	186.34	80.07	3253.23	301.23	7.62	29.555	21.023
	Shatan	32	NJ-32-1d	135	338.3	167.15	2692	599.76	3.01	30.567	20.365
	Shatan	39	NJ-39-1d	193.9	709.9	158.37	784.6	499.37	26.28	29.951	20.786
	–	–	Mean ($n=3$)	205.39	411.51	135.2	2243.28	466.79	12.3	30.024	20.725

sodes of dolomite infilling are significantly lighter. The value of the D1 ranges from −10.15 to −9.29‰, with a mean value of −9.65‰. The value of the D2 ranges from −10.10 to −9.39‰, with a mean value of −9.78‰. Oxygen isotope compositions of two episodes of dolomite infilling are similar.

Strontium isotopes The $^{87}Sr/^{86}Sr$ value of global Cambrian limestone is 0.7095 ± 0.0005, whereas the $^{87}Sr/^{86}Sr$ value of typical Cambrian seawater is 0.7090 ± 0.0002 (Veizer et al. 1999). The D0 of the Longwangmiao Formation has a higher $^{87}Sr/^{86}Sr$ value, which ranges from 0.71096677 to 0.71638223, with a mean value of 0.713010415. The $^{87}Sr/^{86}Sr$ value of D1 ranges from 0.7127816 to 0.71644555, with a mean value of 0.71468714. The $^{87}Sr/^{86}Sr$ value of D2 ranges from 0.71212177 to 0.71406447, with a mean value of 0.712978117 (Table 4).

Discussion

Diagenetic environment of dolomite infilling

The Na and K contents can be used as an indicator of environmental salinity during dolomite diagenesis. The lower the content is, the lower the salinity is and vice versa (Morrow 1982; Warren 2000). The Fe and Mn contents are directly related to dolomite diagenesis. Fe and Mn have a higher electrical charge in the surface oxidizing environment (i.e., Fe^{3+} and Mn^{3+}), and have difficulty entering the dolomite lattice, giving rise to low Fe and Mn contents in dolomite. During the process of burial diagenesis, the fluid becomes reducing, and Fe and Mn take on a lower valency charge (i.e., Fe^{2+} and Mn^{2+}), such that they readily enter the dolomite crystal lattice, which is conducive to the enrichment of Fe and Mn (Brand and Veizer 1981). Owing to the large ionic radius of Ba^{2+}, it has difficulty entering the crystal lattice of dolomite, such that the Ba contents in normal sedimentary dolomite is generally low and with a restricted range. However, hydrothermal fluids have higher Ba content; thus, more Ba is available to enter the dolomite crystal lattice at higher temperatures. Therefore, carbonate minerals formed from hydrothermal fluids will have higher Ba contents (Cai et al. 2008).

D0 in the Longwangmiao Formation has high Na and K contents, low Fe and Mn contents, and relatively low Sr content, indicating that D0 formed from concentrated seawater with high salinity. This may occur in the oxidizing environment near or open to the surface, dolomitization processes are associated with seawater reflux. The Na and K contents in D1 and D2 are lower than that in D0, indicating that the type of fluid differs from concentrated seawater. The salinity is relatively low, indicating the influence of meteoric water. In addition, D1 has higher Fe and Mn contents than D0, which indicates that it is formed in a relative reducing environment. D2 has higher Mn content and lower Fe contents than D0, which indicates that D2 was formed in a relatively oxidizing environment. Meanwhile, there is

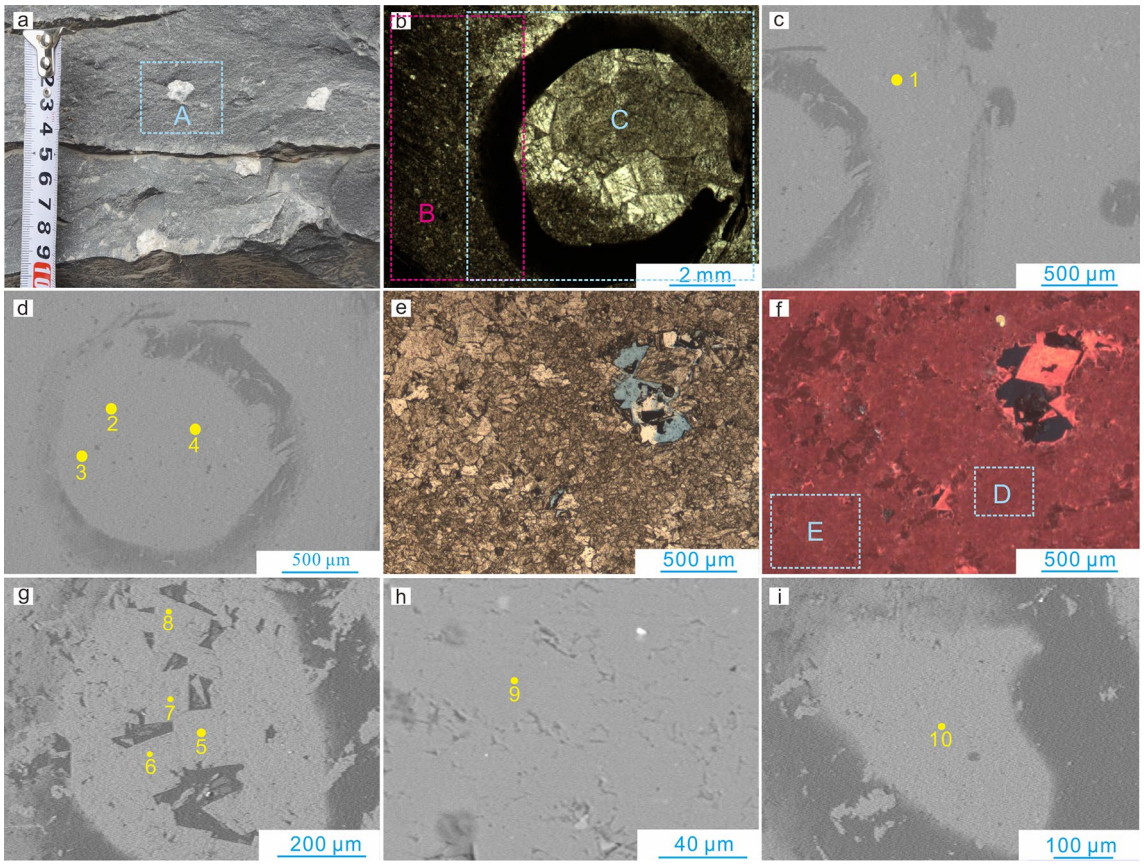

Fig. 6 CL characteristics and electron microprobe point locations of the host dolomite and dolomite infilling in the Longwangmiao Formation, northwestern Sichuan Basin. **a** Outcrop characteristics of D1 in the karst pore-caves; **b** characteristics of D1 in the pore-caves (see the blue dashed box in **a** for the location); **c** electron microprobe point on D0, BSE; **d** electron microprobe point on D0 (see the blue dotted box C in **b**), BSE; **e** characteristics of karst pore-cave infilling; **f** CL characteristics of D2 in the karst pore-caves; **g** electron microprobe point on D2; **h** electron microprobe point on D0 (see **f** for the location in the pink dotted box D), BSE; **i** electron microprobe point on D0 (see **f** for the location of the pink dashed box E), BSE. All samples were taken from the Shatan section. **a**–**e** are from Bed 27 and **f**–**i** are from Bed 44

Table 2 Electron probe analyses of the host dolomite and two episodes of dolomite infilling of the Longwangmiao Formation, northwestern Sichuan Basin

Type	Point	Na_2O (%)	K_2O (%)	FeO (%)	MnO (%)	SrO (%)	MgO (%)	CaO (%)	BaO (%)	Al_2O_3 (%)	SiO_2 (%)	Total (%)
D0	1	0.037	0.057	0.303	0.043	0	22.03	29.55	0	0.117	0.424	52.57
	9	0.069	0.036	0.167	0.051	0.039	22.31	30.115	0	0.011	0.127	52.924
	10	0.063	0.06	0.371	0.017	0	22.269	29.673	0.016	0.216	0.549	53.234
D1	2	0.027	0.002	0.964	0.087	0.028	22.026	29.743	0	0	0.008	52.885
	3	0.021	0.007	0.966	0.024	0.262	22.068	29.646	0	0	0.085	53.079
	4	0.013	0.008	0.534	0.047	0	22.224	29.801	0	0.01	0	52.637
D2	5	0.019	0	0.002	0.012	0.078	22.627	29.843	0.004	0	0.039	52.624
	6	0.025	0.002	0.007	0.068	0	20.779	30.144	0	0	0.041	51.066
	7	0.041	0	0	0.127	0	22.337	29.887	0	0	0.025	52.417
	8	0.045	0.008	0	0.051	0.066	22.46	30.153	0	0.016	0	52.799

no significant difference in Ba and REEs contents between D0 and the two episodes of dolomite infilling, and the two episodes observed in the thin sections exhibit no wavy extinction characteristics under polarized light, indicating that there is no significant relationship with hydrothermal fluids. Therefore, the two episodes of dolomite infilling

Table 3 Element concentrations and ratios for the host dolomite and two episodes of dolomite infilling of the Longwangmiao Formation, northwestern Sichuan Basin

Type	Section/well	Bed/depth (m)	Sample	ΣREE (ppm)	LREE (ppm)	HREE (ppm)	$(Nd/Yb)_{SN}$	δEu	δCe
D0	MS1	7297.85	M1w	23.865	21.208	2.657	1.209	0.881	0.904
	Shatan	27	NJ-27-0C	25.474	22.408	3.066	0.913	1.004	0.955
	Shatan	39	NJ-39-1C	44.904	40.211	4.693	1.420	0.828	1.016
	Shatan	34	NJ-34-00C	25.317	22.405	2.913	0.991	0.908	1.047
	Shatan	32	NJ-32-1C	30.971	27.438	3.533	1.026	1.000	1.025
	Shatan	25-2	NJ-25-2C	52.496	46.607	5.888	1.273	0.903	0.937
	Shatan	25-1	NJ-25-1C	37.598	33.205	4.393	0.814	0.974	0.913
		–	Mean ($n=7$)	34.375	30.498	3.878	1.092	0.928	0.971
D1	Shatan	25-2	NJ-25-2d	40.812	38.618	2.194	3.447	2.792	0.851
	Shatan	25-1	NJ-25-1d	42.495	40.230	2.265	3.469	2.930	0.846
	Shatan	27	NJ-27d	32.228	30.209	2.019	2.567	1.833	0.844
	Shatan	34	NJ-34-00d	32.877	30.733	2.144	2.529	1.827	0.880
	Shatan	34	NJ-34-1d	22.160	20.848	1.312	3.038	1.979	0.888
		–	Mean ($n=5$)	34.114	32.127	1.987	3.010	2.272	0.862
D2	MS1	7297.85	M1m	126.802	119.730	7.073	3.876	0.855	0.919
	Shatan	32	NJ-32-1d	52.438	47.966	4.471	1.965	0.979	0.881
	Shatan	39	NJ-39-1d	56.072	50.612	5.460	1.761	0.987	0.980
		–	Mean ($n=3$)	78.437	72.769	5.668	2.534	0.940	0.926

$\delta Eu = 2(Eu/Eu_{shale})/(Sm/Sm_{shale} + Gd/Gd_{shale})$; $\delta Ce = 2(Ce/Ce_{shale})/(La + La_{shale} + Pr/Pr_{shale})$ (Haskin and Haskin 1966)

Table 4 Results of carbon, oxygen, and strontium isotopes of the host dolomite and two episodes of dolomite infilling in the Longwangmiao Formation, northwestern Sichuan Basin

Type	Section/well	Bed/depth	Sample	$\delta^{13}C_{PDB}$ (‰)	Mean $\delta^{13}C_{PDB}$ (‰)	$\delta^{18}O_{PDB}$ (‰)	Mean $\delta^{18}O_{PDB}$ (‰)	$^{87}Sr/^{86}Sr$	Error (2σ)	Mean $^{87}Sr/^{86}Sr$
D0	MS1	7302.6 m	M5w	−1.05	−0.36	−4.89	−6.07			0.713010415
	Shatan	25	NJ-25-1	0.48		−6.28		0.71638223	8.39×10^{-5}	
	Shatan	27	NJ-27	0.64		−6.39		0.71349904	7.33×10^{-5}	
	Shatan	32	NJ-32-1	−0.15		−6.21				
	Shatan	35	NJ-35-1	−1.4		−6.53		0.71386677	2.64×10^{-5}	
	Shatan	35	NJ-35-2	−1.27		−5.23		0.71096608	1.26×10^{-4}	
	Shatan	37	NJ-37-1	0.3		−6.86		0.71225017	4.07×10^{-5}	
	Shatan	39	NJ-39-1	−0.42		−6.14		0.7110982	7.74×10^{-5}	
D1	Shatan	25	NJ-25-1D	0.41	−0.18	−10.15	−9.65	0.71644555	3.19×10^{-5}	0.71468714
	Shatan	27	NJ-27D	0.68		−9.51		0.71483427	6.41×10^{-5}	
	Shatan	34	NJ-34-00D	−0.77		−9.29		0.7127816	3.84×10^{-5}	
	Shatan	34	NJ-34-01D	−1.03		−9.63				
D2	Shatan	39	NJ-39-1D	−1.22	−0.96	−9.39	−9.78	0.71212177	1.19×10^{-4}	0.712978117
	Shatan	37	NJ-37-1D	−1.05		−10.1		0.71274811	4.41×10^{-5}	
	Shatan	35	NJ-35-1D	−1.02		−9.79		0.71406447	6.34×10^{-4}	
	Shatan	32	NJ-32-1D	−0.29		−9.6				
	MS1	7302.6 m	M5m	−1.21		−10				

may be affected by meteoric water, but with a weaker first stage.

The ^{87}Sr isotope is generally derived from the decay of the radioactive element Rb; therefore, its abundance changes with time. Meanwhile, ^{86}Sr is not radioactive, and its abundance is relatively stable. Clastic rocks and mudstones usually contain more of the radioactive ^{87}Sr and have higher $^{87}Sr/^{86}Sr$ values. Longwangmiao Formation is mixed with a

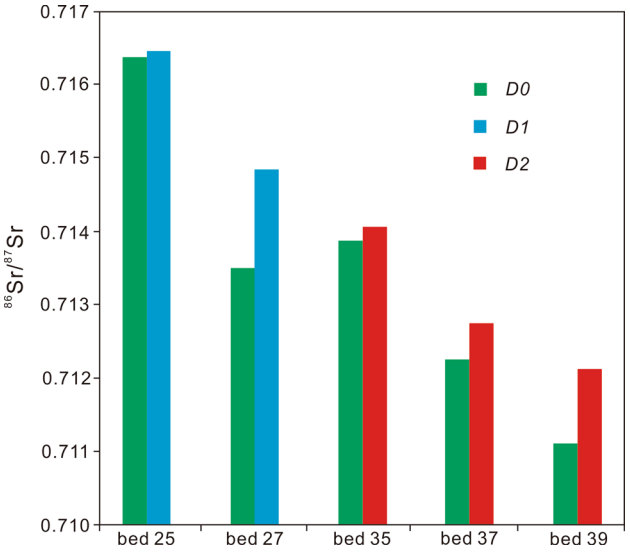

Fig. 7 The $^{87}Sr/^{86}Sr$ values of dolomite and two episodes of dolomite infilling in the Longwangmiao Formation, northwestern Sichuan Basin

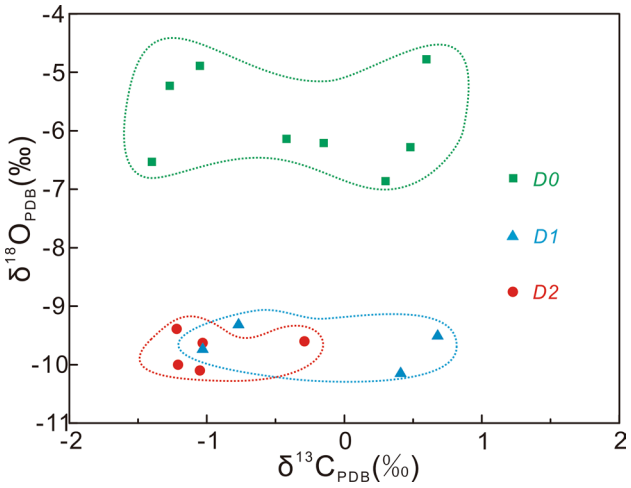

Fig. 8 Carbon and oxygen isotope characteristics of dolomite and the two episodes of dolomite infilling in the Longwangmiao Formation, northwestern Sichuan Basin

large amount of terrestrial detritus, such that D0 has higher $^{87}Sr/^{86}Sr$ values. Meanwhile, the distribution of $^{87}Sr/^{86}Sr$ values of the two episodes of dolomite infilling are higher than that of D0 of the same layer (Table 3, Fig. 7). Which implies that there is no effect of deeper mantle-derived fluids. Otherwise, it also shows that the formation water, which was preserved in the syngenetic karstification of Longwangmiao Formation is strongly influenced by the terrigenous clastic rocks in the non-synsedimentary stratum. The characteristics of the strontium isotope indicated that D1 and D2 were not affected by hydrothermal activity, whereas meteoric water was involved.

The dissolution and recrystallization of the carbonaceous minerals in the strata do not result in significant differences in the carbon isotopic of carbonate precipitation; however, the carbon from different sources has a significant impact on their isotopes (Talma and Netterberg 1983). The carbon isotopic composition of carbonate precipitation is affected by CO_2 in meteoric water and from organic sources (Irwin and Curtis 1977; Lomann 1988). Compared with carbon isotope, oxygen isotope is more likely to be affected and shifted (Banner and Hanson 1990), the oxygen isotopes of the precipitated dolomite are lighter, indicating that the fluid is mixed with meteoric water or formed at a higher temperature (Zhu et al. 2013). The value of $\delta^{13}C$ in D1 has a similar to that in D0, possibly because much of the original marine carbon information was preserved in a relatively closed reduction environment. While the value of $\delta^{13}C$ in D2 is lighter than that in D0, it may form in a relatively open environment, resulting in the scenario in which ^{12}C-enriched meteoric water enters the stratum quickly. The value of $\delta^{18}O$ in D1 and D2 is lighter than that in D0, which indicates that the two episodes of dolomite infilling may have been affected by the meteoric water factors (Fig. 8).

The composition of REEs in carbonate rocks is mainly controlled by physical and chemical conditions and the REEs in the fluid during mineral precipitation (Bau and Möller 1992). REEs in fluids may be derived from rocks that interact with the fluids (Zhu et al. 2013). The characteristics of REEs in the rocks interacting with the fluids determine the content and composition of the REEs in the fluids, which are also influenced by the characteristics of the fluid-rock interactions and the types and concentrations of the complexing ions in the fluids (Warmada et al. 2007). Eu anomalies are directly affected by redox conditions to a large extent. Even at low temperature and in near-surface environments, Eu^{2+} can be abundant in reduced fluids (Sverjensky 1984; Bau 1991; MacRae et al. 1992). As Eu^{2+} and Ca^{2+} have the same electrical charge and similar ionic radii, Eu can easily replace Ca^{2+} in dolomite, leading to the occurrence of a positive Eu anomaly.

D1 shows LREE enrichment and slight HREE depletion (Fig. 9a). Clastic rocks usually have LREE enrichment, thus, the fluids may have strong water–rock interactions with the clastic rocks, causing the REEs to dissolve in the fluids, and resulting in high REE contents and enrichment of LREEs in precipitated dolomite during this stage. In addition, the precipitated dolomite in this stage exhibits positive Eu and weak negative Ce anomalies relative to the host rocks, indicating that the fluid environment exhibited relatively reducing conditions. The distribution of REEs in D2 is basically the same as that of the D0 (Fig. 9b), which indicates that the REE characteristics of the fluids in this stage were inherited from D0

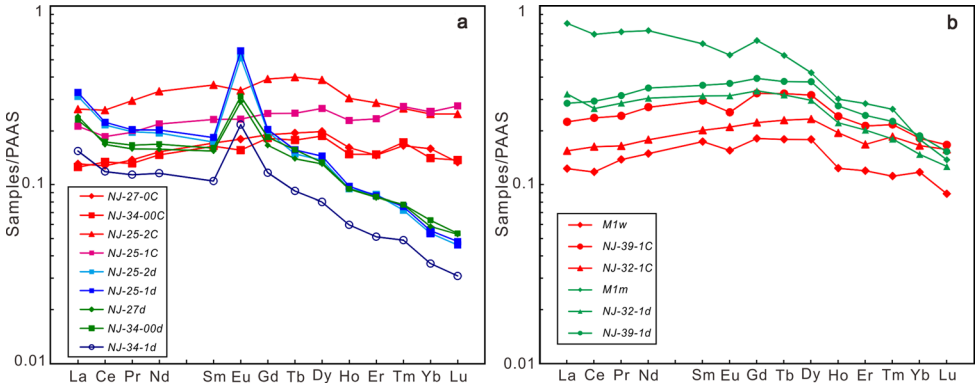

Fig. 9 NASC-normalized REE patterns of the host dolomite and two episodes of dolomite infilling in the Longwangmiao Formation, northwestern Sichuan Basin. **a** Comparison of REE pattern between D0 and D1; **b** comparison of REE pattern between D0 and D2. Values of NASC are from Taylor and McLennan (1985)

and were extracted from the dolomite during the process of water–rock interaction. At this stage, the precipitated dolomites have relatively weak negative Eu anomalies, indicating that the fluid environment in this stage was a relatively open oxidizing environment.

In general, based on the systematic analyses of elements and isotopes, we conclude that both episodes of infillings have been affected by meteoric water and have not been altered by hydrothermal fluids. Compared with the second episode infilling, the first episode infilling takes place in a relatively closed environment.

Geological process of dolomite fluid infilling

During the process of repeated subaerial exposure of grain shoals in the penecontemporaneous stage, erosion marks are often formed on the surface of the layers, primarily because of the scouring of unconcentrated flow and overflow, which belongs to an unrestricted flow regime (Zhang et al. 2016). A series of layered dissolution pore-caves are formed, but at a relatively small scale, typically forming mold pores and intragranular dissolution pore-caves. Under hot arid climatic conditions, evaporation is intense, and surface seawater or pore water is continuously concentrated and salinized, forming a brine with high Mg^{2+}/Ca^{2+} values and resulting in the dolomitization of the host sediments (Fig. 10a, b). After burial, the dissolution pore-caves are infilled with dolomite (Fig. 10c, d).

In the shallow burial stage, meteoric water infiltrating downward may have fully interacted with the clastic rocks of the overlying Douposi Formation (Fig. 10c). The meteoric water was already in a relatively closed reducing

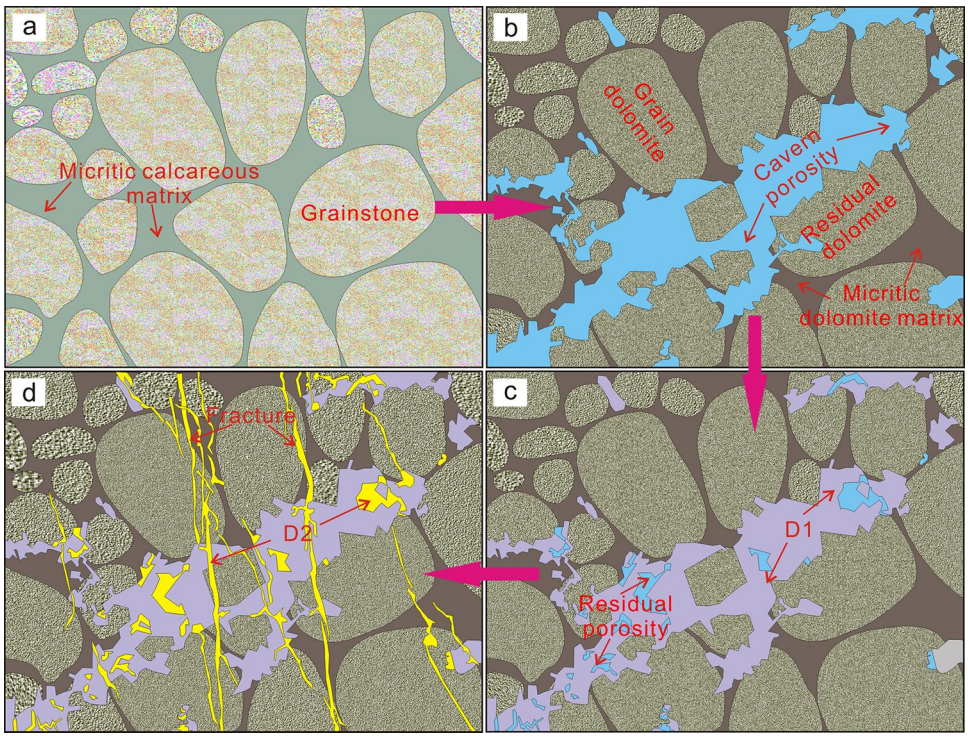

Fig. 10 The sequence of karst pore-cave dolomite infilling in the Longwangmiao Formation, northwestern Sichuan Basin. **a** Depositional stage; **b** dissolution pore-caves are formed, syngenetic stage; **c** the stage of karst pore-cave infilled by D1 at the shallow burial stage; **d** the stage of karst fracture-vug infilled by D2 during the Caledonian–Hercynian period

environment when it entered the Longwangmiao Formation in the process of continuous infiltration; then, the water mixed with connate water and continued to interact with D0. After the solubility of dolomite reached saturation and oversaturation, D1 would have precipitated in the karst pores and caves that formed in the eogenetic stage (Fig. 11a). Therefore, the REE pattern of D1 is characterized by a pattern of clastic rocks and a relatively strong positive Eu anomaly.

The fluid properties of D2 are consistent with high angle fractures. Field observation showed that the high-angle fractures in this stage are tensile fractures. Meanwhile, the microscopic features show that the formation of the tensional fractures take palce earlier than the infilling of the residual voids with organic matter. The lower Cambrian hydrocarbon source rocks began large-scale hydrocarbon generation and migration in the Middle Permian to Middle Triassic, combined with the burial history of the lower Cambrian strata in the northwestern Sichuan Basin (Fig. 3), the timing of the D2 of fracture-vugs was restricted to the period before the Permian, corresponding to the Caledonian–Hercynian period. Caledonian–Hercynian tectonic movements heavily affected the northwestern Sichuan Basin. A series of high-angle fractures were formed in the Longwangmiao Formation. As the fractures may have corresponded to a relatively open system, meteoric water permeated rapidly into the Longwangmiao Formation through the fractures, resulting in only weak water–rock interactions with the overlying clastic rocks. When the meteoric water entered the Longwangmiao Formation, it mixed with the connate water and interacted with D0. When the solubility of the dolomite reached saturation and oversaturation, D2 would have precipitated (Fig. 11b). Therefore, the REE pattern of D2 in the fracture-caves inherited the characteristics of the host rock.

After the second episode of dolomite infilling of the fracture-vugs (Fig. 10d), the small karst pore-caves formed by the syngenetic karstification, primarily in the shoal, have been compacted. During the Middle Permian to Middle Triassic, the lower Cambrian source rocks generated and migrated large volumes of hydrocarbons, and the organic matter filled into the residual pore-caves.

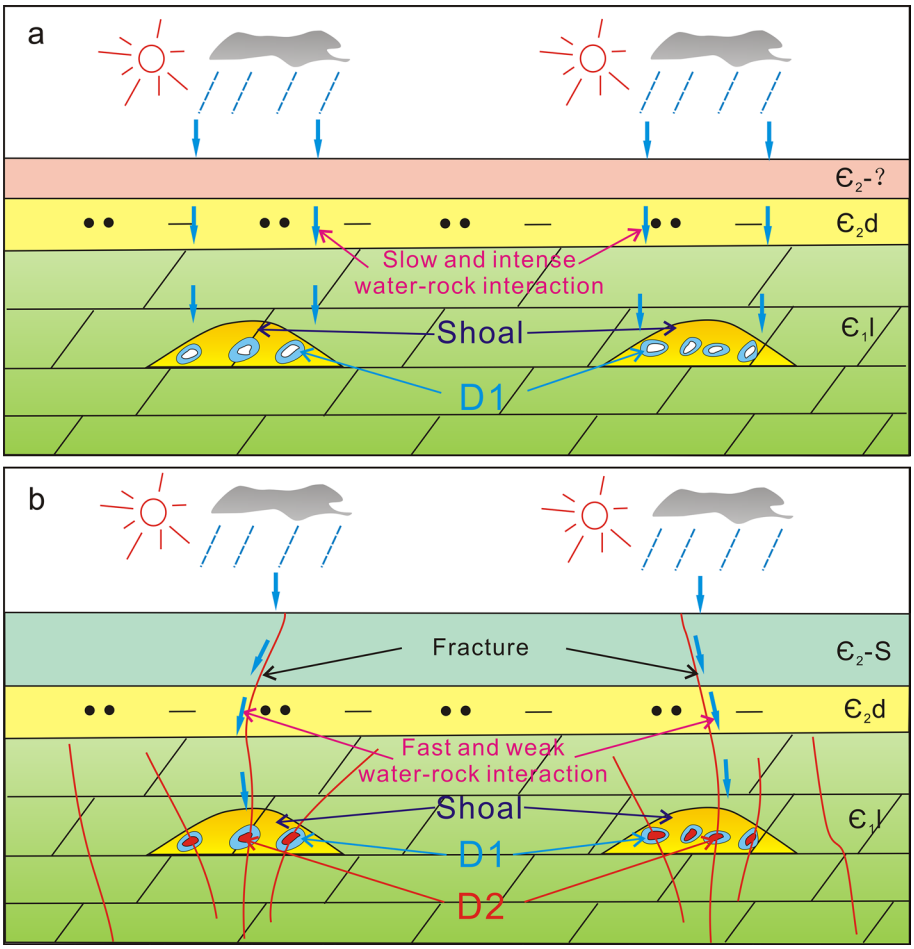

Fig. 11 Model diagram of the infilling process of the Longwangmiao Formation karst reservoir in the northwestern Sichuan Basin. **a** The D1 infilling process; **b** the D2 infilling process

Significance for the hydrocarbon exploration of Longwangmiao Formation in northwestern Sichuan Basin

According to the in-situ experimental simulation of the burial process of carbonate rocks, it is believed that the deep carbonate reservoir is mainly formed by an open system with near surface conditions, i.e., intergranular pores formed in the sedimentary period, and dissolution pores formed near the surface (Yang et al. 2014). However, the burial process is generally a process of gradual closure and the deacceleration of the fluid exchange; this process is mainly destructive and harmful to reservoir. Therefore, it is considered that the target of exploration of the carbonate rocks is to located the reservoir that was formed in the eogenetic stage and diagenetic evolution, constructive for pore preservation (Ma et al. 2017).

Syngenetic and penecontemporaneous karstification is the key to the reservoir in Longwangmiao Formation of the central Sichuan Basin (Liu et al. 2014b; Zhang et al. 2015; Zhou et al. 2015). In the subsequent burial process, the superimposition by Caledonian–Hercynian supergene karstification resulted in the formation of a high-quality reservoir (Jin et al. 2014; Yang et al. 2015). In the Longwangmiao Formation of the northwestern Sichuan Basin, a large set of dissolution pore-caves ranging in size from several millimeters to several centimeters formed by the karstification during the eogenetic stage, providing a good foundation for reservoir formation, similar to the Longwangmiao Formation of the central Sichuan Basin. However, during the burial process, those dissolution pore-caves were generally filled with the two dolomite episodes (D1 and D2). The filling of hydrocarbon and organic acid can inhibit the damage of cementation to the pores formed in the early stage during process of burial; thus, it is beneficial to the maintenance of pores (Ma et al. 2019). However, our research results show that the two episodes of dolomite infilling occurred before the formation and migration of hydrocarbons. Therefore, the dissolution pore-caves formed in the syngenetic stage were generally compacted during the massive hydrocarbon migration of the Lower Cambrian source rocks which occurred in the Middle Permian to Middle Triassic. The Longwangmiao Formation in the well MS1 and Shatan section are different from that in the central Sichuan Basin, which lacks the alteration of the supergene karstification during the Caledonian–Hercynian period (Jin et al. 2014; Yang et al. 2015; Zhang et al. 2015; Du et al. 2016; Zhou et al. 2016). In addition, buried dissolution is considered to be an important diagenesis supplement to the development and maintenance of deep reservoir space (Surdam et al. 1984; Mazzullo and Harris 1992; Moore 2001b). However, based on the well MS1 and Shatan section, the buried dissolution diagenesis is not developed in the Longwangmiao Formation.

Therefore, during the continuous burial process after the formation of the dissolution pore-caves, which were formed by eogenetic karstification in the Longwangmiao Formation, the major mechanism leading to the degradation of the carbonate reservoir space is the precipitation from the two episodes of dolomite infilling. The eogenetic karst reservoir of the Middle-Lower Ordovician strata in Shunnan, northern slope of Tazhong uplift, Tarim Basin, presented densification to be significantly filled with subsequent carbonate cementation, whereas the hydrocarbon exploration target is where the later karst area is superimposed (Chen et al. 2016). The situation is the same as in the eogenetic karst reservoir of Longwangmiao Formation in the central Sichuan Basin. Based on the results of the comprehensive study, we can determine that the eogenetic karst reservoir is easy to be compacted by destructive diagenesis (e.g., carbonate cementation) during the burial process, and the favorable reservoir space needs to be superimposed by other's constructive diagenesis (e.g., superimposed by the later karst). The area in the southern of Shatan section-Well MS1, closed to the paleo-uplift of the central Sichuan Basin, where the slope of karstification during the Caledonian–Hercynian period is located, exhibits the eogenetic karstification of the Longwangmiao Formation superimposed by the Caledonian–Hercynian supergene karstification. Which would be beneficial for formation of the effective reservoir, and is the focus area for finding potential reservoirs in the future.

Conclusions

1. In the Cambrian Longwangmiao Formation of the northwestern Sichuan Basin, a large set of dissolution pore-caves ranging in size from several millimeters to several centimeters developed in the interior of the dolomite, and were formed by syngenetic karstification in the eogenetic stage. The episodic change in the sea level is the key to the formation of the dissolution pore-caves during the eogenetic stage. Meanwhile, the major mechanism leading to the degradation of the reservoir space is the precipitation of two episodes of dolomite during the continuous burial process after dissolution.
2. The geochemical data indicate two episodes of dolomite infilling (D1 and D2), which were affected by meteoric water in the shallow burial stage. The downward infiltration of meteoric water may have had sufficient water–rock interaction with the clastic rocks of the overlying Douposi Formation, such that it would already have been in a relatively closed reducing environment upon entering the Longwangmiao Formation. Owing to the relatively open system of fractures during the Caledonian–Hercynian period and the rapid penetration of meteoric water down to the Longwangmiao Formation

through the fractures, the precipitated dolomite exhibits characteristics of precipitation in a relatively oxidizing environment.

3. The favorable eogenetic karst reservoir needs to be superimposed by other constructive diagenesis, as it is easily filled with carbonate cementation in the later burial process. The area that is located in the southern of Shatan section-Well MS1 of the northwestern Sichuan Basin is close to the paleo-uplift of the central Sichuan Basin area, which may be superimposed by the supergene karstification during the Caledonian–Hercynian period; as such, it would be a favorable area to exploration.

Acknowledgements This work was supported by the National Natural Science Foundation of China (Grant Nos. 41872137 and 40739903). We sincerely thank the senior engineer Peiquan Kang, Prof. Kun Deng, and Prof. Ziliang Liu from Chengdu University of Technology for the field investigation. We also thank Prof. Jingyong Xu, Dr. Di Yang, Huaixing Yang, Zehua Niu, and Jin Zhang from the Chengdu University of Technology for the carbon and oxygen isotope, strontium isotope, and major and trace elements analyses.

References

Baceta JI, Wright VP, Beavington-Penney SJ, Pujalte V (2007) Palaeohydrogeological control of palaeokarst macro-porosity genesis during a major sea-level lowstand: Danian of the Urbasa-Andia plateau, Navarra, North Spain. Sed Geol 199:141–169

Banner JL, Hanson GN (1990) Calculation of simultaneous isotopic and trace element variations during water–rock interaction with applications to carbonate diagenesis. Geochim Cosmochim Acta 54:3123–3137

Bau M (1991) Rare-earth element mobility during hydrothermal and metamorphic fluid-rock interaction and the significance of the oxidation state of europium. Chem Geol 93:219–230

Bau M, Möller P (1992) Rare earth element fractionation in metamorphogenic hydrothermal calcite, magnesite and siderite. Mineral Petrol 45:231–246

Brand U, Veizer J (1981) Chemical diagenesis of a multicomponent carbonate system-I: trace elements. J Sediment Petrol 50:1219–1236

Budd AD, Saller AH, Harris PM (1995) Unconformities and porosity in Carbonate strata. AAPG Memoir 63:313

Cai CF, Li KK, Li HT, Zhang BS (2008) Evidence for cross formational hot brine flow from integrated $^{87}Sr/^{86}Sr$, REE and fluid inclusions of the Ordovician veins in Central Tarim, China. Appl Geochem 23:2226–2235

Chen HH, Wu Y, Zhu HT, Lu ZY, Cao ZC, Yun L (2016) Eogentic karstification and reservoir formation model of the Middle-Lower Ordovician in the northeast slope of Tazhong Uplift, Tarim Basin. Acta Petrolei Sinica 37:1231–1246 **(in Chinese with English abstract)**

Choquette PW, Pray LC (1970) Geologic nomenclature and classification of porosity in sedimentary carbonates. Am Asso Petrol Geol Bull 54:207–250

Craig DH (1988) Caves and other features of Permian karst in San Andres dolomite, Yates Field reservoir, west Texas. In: James NP, Choquette PW (eds) Paleokarst. Springer, New York, pp 342–363

Cunningham KJ, Florea LJ (2009) The Biscayne Aquifer of Southeastern Florida. J Geophys Res 65:196–199

Dai LC, Wang XZ, Du SY, Yang XF, Yang YM (2016) Characteristics and genesis of Lower Cambrian Longwangmiao shoal-facies reservoirs in central part of Sichuan Basin. Marine Origin Petroleum Geology 21:19–28 **(in Chinese with English abstract)**

Dan Y, Lin LB, Liang B, Zhang QY, Yu Y, Cao JW, Li JR (2018) Eogenetic karst control of carbonate reservoirs during a transient exposure: a case study of the Ordovician Yingshan Formation in the northern slope of the Tazhong Uplift, Tarim Basin. China Minerals 8:345

Demiralin AS, Hurley NF, Oesleby TW (1993) Karst breccias in the Madison limestone (Mississippian), Garland field, Wyoming. In: Fritz RD, Wilson JL, Yurewicz DA (eds) Paleokarst related hydrocarbon reservoirs. Society for Sedimentary Geology, New Orleans, pp 101–118

Du JH, Zhang BM, Wang ZC, Zou CN, Xu CC, Shen P, Zhang J, Zhang J, Zhou H, Jiang H, Wen L, Shan XQ, Liu JJ (2016) Sedimentary model and reservoir genesis of dual grain banks at the Lower Cambrian Longwangmiao Fm carbonate ramp in the Sichuan Basin. Nat Gas Ind 36:1–10 **(in Chinese with English abstract)**

Feng ZZ, Peng YM, Jin ZK, Jiang PL, Bao ZD, Luo Z, Ju TY, Tian HQ, Wang H (2001) Lithofacies palaeogeography of the Cambrian in South China. J Palaeogeogr 3:1–14 **(in Chinese with English abstract)**

Feng WM, Xie Y, Liu JQ, Wang ZJ, Lin JS, Huang XP (2014) Sedimentary model and hydrocarbon exploration targets of the Lower Cambrian Longwangmiao Formation in the Upper Yangtze area. Geol Sci Technol Inf 33:106–111

Grimes KG (2006) Syngenetic Karst in Australia: a review. Helictite 39:27–38

Gu ZD, Yin JF, Jiang H, Zhang BM, Li QF, Yuan M, Zhai XF, Zhang L, Yang F (2016) Tectonic evolution from Late Sinian to Early Paleozoic and natural gas exploration in northwestern Sichuan Basin, SW China. Petrol Explor Dev 43:1–12

Hardage BA, Carr DL, Lancaster DE, Simmons JL Jr, Elphick RY, Pendleton VM, Johns RA (1996) 3-D seismic evidence of the effects of carbonate karst collapse on overlying clastic stratigraphy and reservoir compartmentalization. Geophysics 61:1336–1350

Hardie LA, Bosellini A, Goldhammer RK (1986) Repeated subaerial exposure of subtidal carbonate platforms, Triassic, northern Italy: evidence for high frequency sea level oscillations on a 10^4 year scale. Paleoceanography 1:447–457

Haskin MA, Haskin LA (1966) Rare earths in European shales: a redetermination. Science 154:507–509

Irwin H, Curtis C (1977) Isotopic evidence for source of diagenetic carbonates formed during burial of organic rich sediments. Nature 15:209–213

James NP, Choquette PW (1988) Paleokarst. Springer, Berlin

Jin MD, Zeng W, Tan XC, Li L, Li ZY, Luo B, Zhang JL, Liu JW (2014) Characteristics and controlling factors of beach-controlled karst reservoirs in Cambrian Longwangmiao Formation, Moxi-Gaoshiti area, Sichuan Basin, NW China. Petrol Explor Dev 41:712–723

Liu SG, Deng B, Li ZW, Sun W (2012) Architecture of basin-mountain systems and their influences on gas distribution: a case study from the Sichuan basin, South China. J Asian Earth Sci 47:204–215

Liu SG, Ma YS, Wang GZ, Cai XY, Xu GS, Sun W (2014a) Formation process and mechanism of the Sinian-Silurian natural gas reservoirs in the Sichuan Basin. Science and Technology Press, Beijing

Liu SG, Song JM, Zhao YH, Zhong Y, Song LK, Tian YH, Liang F, Yin KW, Li JL (2014b) Controlling factor of formation and distribution of Lower Cambrian Longwangmiao Formation high-quality reservoirs in Sichuan Basin, China. J Chengdu Univ Technol (Sci Technol Edn) 41:657–670 **(in Chinese with English abstract)**

Lomann KG (1988) Geochemical patterns of meteoric diagentic systems and their application to studies of paleokarst. Paleokarst. Springer-Verlag, New York, pp 58–80

Loucks RG (1999) Paleocave carbonate reservior: origins, burial-depth modifications, spatial complexity and reservoir implications. AAPG Bull 83:1795–1834

Ma T, Tan XC, Li L, Zeng W, Jin MD, Luo B, Hong HT, Yang Y (2015) Sedimentary characteristics and distribution of grain shoals in the Lower Cambrian Longwangmiao Formation of Sichuan Basin and its adjacent areas. J Palaeogeogr 17:213–228 **(in Chinese with English abstract)**

Ma YS, He DF, Cai XY, Liu B (2017) Distribution and fundamental science questions for petroleum geology of marine carbonate in China. Acta Petrol Sinica 33:1007–1020 **(in Chinese with English abstract)**

Ma YS, He ZL, Zhao PR, Zhu HQ, Han J, You DH, Zhang JT (2019) A new progress in formation mechanism of deep and ultra-deep carbonate reservoir. Acta Petrol Sinica 40:1415–1425 **(in Chinese with English abstract)**

MacRae ND, Nesbitt HW, Kronberg BI (1992) Development of a positive Eu anomaly during diagenesis. Earth Planet Sci Lett 109:585–591

Mazzullo SJ, Harris PM (1992) Mesogenetic dissolution: Its role in porosity development in carbonate reservoirs. AAPG Bull 76:607–620

McDonnell A, Loucks RG, Dooley T (2007) Quantifying the origin and geometry of circular sag structures in northern Fort Worth Basin, Texas: paleocave collapse, pull-apart fault systems, or hydrothermal alteration? AAPG Bull 91:1295–1318

Moore CH (2001a) Carbonate reservoirs: porosity evolution and diagenesis in a sequence stratigraphic framework: developments in sedimentology. Elsevier, New York

Moore CH (2001b) Carbonate diagenesis and porosity. Elsevier, New York

Moore PJ, Martin JB, Screaton EJ, Nuehoff PS (2010) Conduit enlargement in an eogenetic karst aquifer. J Hydrol 393:143–155

Morrow DW (1982) Diagenesis 2. Dolomite-Part 2: dolomite models and ancient dolostones. Geosci Can 9:5–13

Nicolas C, Immenhauser A, Amour F, Mutti M, Preston R, Whitaker FF, Peterhäsel A, Egenhoff SO, Dunn PA, Agar SM (2012) Triassic Latemar cycle tops—subaerial exposure of platform carbonates under tropical arid climate. Sed Geol 265–266:1–29

Nothdurft LD, Webb GE, Kamber BS (2004) Rare earth element geochemistry of Late Devonian reefal carbonates, Canning Basin, Western Australia: Confirmation of a seawater REE proxy in ancient limestones. Geochim Cosmochim Acta 68:263–283

Rao S, Zhu CQ, Wang Q, Tang XY, Li WW, Jiang GZ, Hu SB, Wang JS (2013) Thermal evolution patterns of the Sinian-Lower Paleozoic source rocks in the Sichuan Basin, Southwest China. Chin J Geophys 56:1549–1559

Ren Y, Zhong DK, Gao CL, Liang T, Sun HT, Wu D, Zheng XW (2017) High-resolution carbon isotope records and correlations of the lower Carbrian Longwangmiao formation (stage 4, Toyonian) in Chongqing, South China. Palaeogeogr Palaeoclimatol Palaeoecol 485:572–592

Richardson NJ, Densmore AL, Seward D, Fowler A, Wipf M, Ellis MA, Li Y, Zhang Y (2008) Extraordinary denudation in the Sichuan Basin: Insights from low-temperature thermochronology adjacent to the eastern margin of the Tibetan Plateau. J Geophys Res 113:B04409

Surdam RC, Boese SW, Crossey LJ (1984) The chemistry of secondary porosity. AAPG Memoir 37:127–150

Sverjensky DA (1984) Europium redox equilibria in aqueous solution. Earth Planet Sci Lett 67:70–78

Talma AS, Netterberg F (1983) Stable isotope abundance in calcretes. Geol Soc Lond Special Publ 11:221–233

Tan XC, Xiao D, Chen JS, Li L, Liu H (2015) New advance and enlightenment of eogenetic karstification. J Palaeogeogr 17:441–456 **(in Chinese with English abstract)**

Taylor SR, Mclenan SM (1985) The continental crust: its composition and evolution. Blackwell, London

Torsvik TH, Cocks LRM (2013) New global palaeogeographical reconstructions for the early Palaeozoic and their generation. Geol Soc Lond Memoirs 38:5–24

Vacher HL, Mylroie JE (2002) Eogenetic karst from the perspective of an equivalent porous medium. Carbonates Evaporites 17:182–196

Veizer J, Ala D, Azmy K, Bruckschen P, Buhl D, Bruhn F, Carden GAF, Diener A, Ebneth S, Godderis Y, Jasper T, Korte C, Pawellek F, Podlaha OG, Strauss H (1999) $^{87}Sr/^{86}Sr$, $\delta^{13}C$ and $\delta^{18}O$ evolution of Phanerozoic seawater. Chem Geol 161:59–88

Warmada IW, Lehmann B, Simandjuntak M, Hemes HS (2007) Fluid inclusion, rare-earth element and stable isotope study of carbonate minerals from the Pongkor Epithermal gold-silver deposit, West Java, Indonesia. Res Geol 57:124–135

Warren J (2000) Dolomite: occurrence, evolution and economically important associations. Earth Sci Rev 52:1–81

White S, Webb JA (2015) The influence of tectonics on flank margin cave formation on a passive continental margin: Naracoore, Southeastern Australia. Geomorphology 229:58–72

Xiao D (2017) Research on eogenetic karst of marine carbonate and its reservoir in the three major basin, Western China. Southwest Petroleum University Doctoral Dissertation, Chengdu

Xiao D, Tan XC, Xi AH, Liu H, Shan SJ, Xia JW, Cheng Y, Lian CB (2016) An inland facies-controlled eogenetic karst of the carbonate reservoir in the Middle Permian Maokou Formation, southern Sichuan Basin, SW China. Mar Pet Geol 72:218–233

Yang YK, Liu B, Qin S, Luo P, Zhang SM, Zhou MH, Shi KB, Tian YJ (2014) Re-recognition of deep carbonate dissolution based on the observatuon of in-situ simulation experiment. Acta Scientirum Naturalium Unversitatis Pekinensis 50:317–322 **(in Chinese with English abstract)**

Yang XF, Wang XZ, Dai CL, Yang YM, Xie JR, Luo WJ (2015) Sedimentary features of the Lower Cambrian Longwangmiao Formation in the central Sichuan Basin. Lithol Reservoirs 27:95–101 **(in Chinese with English abstract)**

Yu Q, Mu CL, Zhang HQ, Tan QY, Xi XS, Yan JF (2011) Sedimentary evolution and reservoir distribution of northern Upper Yangtze plate in Sinian-Early Paleozoic. Acta Petrol Sinica 27:672–680 **(in Chinese with English abstract)**

Zhang BM, Liu JJ (2009) Classification and characteristics of karst reservoirs in China and related theories. Petrol Explor Dev 36:12–29

Zhang JY, Luo WJ, Zhou JG, Wang Y, Tang S, Luo B, Pan LY, Ni C, Gu MF, Li WZ (2015) Main origins of high quality reservoir of Lower Cambrian Longwangmiao Formation in the giant Anyue Gasfield, Sichuan Basin, SW China. Nat Gas Geosci 26:2063–2074 **(in Chinese with English abstract)**

Zhang H, Cai ZX, Qi LX, Yun L (2016) Types and characteristics of eogentic karst in the Yingshan Formation in northwestern Tazhong area, Tarim Basin. Oil Gas Geol 37:291–303 **(in Chinese with English abstract)**

Zhao WZ, Shen AJ, Qiao ZF, Zheng JF, Wang XF (2014) Carbonate karst reservoirs of the Tarim Basin, northwest China: types, features, origins, and implications for hydrocarbon exploration. Interpretation 2:SF65–SF90

Zhou JG, Xu CC, Yao GS, Yang G, Zhang JY, Hao Y, Wang F, Pan LY, Gu MF, Li WZ (2015) Genesis and evolution of Lower Cambrian Longwangmian Foramtion reservoirs, Sichuan Basin, SW China. Petrol Explor Dev 42:175–184

Zhou H, Zhang BM, Li W, Shan XQ, Fan JW, Liu JJ, Zhang SB, Wen L, Luo B, Luo WJ (2016) Characteristics and petroleum geological implication of paleo-cave fillings in Longwangmiao Formation of Lower Cambrian in central Sichuan Basin, China. J Chengdu

Univ Technol (Sci Technol Edn) 43:188–198 **(in Chinese with English abstract)**

Zhu MY, Babcock LE, Peng SC (2006) Advances in Cambrian stratigraphy and paleontology: intergrating correlation techniques, paleobiology, taphonomy and paleoenvironmental reconstruction. Palaeoworld 15:217–222

Zhu DY, Meng QQ, Hu WX, Jin ZJ (2012) Deep Cambrian surface karst dolomite reservoir and its alteration by later fuild in Tarim Basin. Geol Rev 58:691–701 **(in Chinese with English abstract)**

Zhu DY, Meng QQ, Hu WX, Jin ZJ (2013) Differences between fluid activities in the Central and Northern Tarim Basin. Geochimica 42:82–94 **(in Chinese with English abstract)**

Zhu DY, Zhang DW, Li SJ, Feng JF, Sun DS, Lin JH, Zhang RQ (2015) Development genesis and characteristics of karst reservoirs in lower assemblage in Sichuan Basin. Mar Origin Petrol Geol 20:33–44 **(in Chinese with English abstract)**

Zhu DY, Zhang DW, Liu QY, Xing FC, He ZL, Zhang RQ, Liu ZH (2018) Formation mechanism of dolomite reservoir controlled by fourth-order sequence in an evaporated marine environment—an example from the Lower Ordovician Tongzi Formation in the Sichuan Basin. Energy Explor Exploit 34:620–644

Zou CN, Du JH, Xu CC, Wang ZC, Zhang BM, Wei GQ, Wang TS, Yao GS, Deng SH, Liu JJ, Zhou H, Xu AN, Yang Z, Jiang H, Gu ZD (2014) Formation, distribution, resource potential and discovery of the Sinian-Cambrian giant gas field, Sichuan Basin, SW China. Petrol Explor Dev 41:306–325